Signature of the Schwinger pair creation rate via radiation generated in graphene by a strong electric current

M. Lewkowicz,[1] H. C. Kao,[2] and B. Rosenstein[3,4,1,*]

[1]*Physics Department, Ariel University Center, Ariel 40700, Israel*

[2]*Physics Department, National Taiwan Normal University, Taipei 11677, Taiwan, Republic of China*

[3]*Electrophysics Department, National Chiao Tung University, Hsinchu 30050, Taiwan, Republic of China*

[4]*National Center for Theoretical Sciences, Hsinchu 30043, Taiwan, Republic of China*

(Received 10 May 2011; published 20 July 2011)

Electron-hole pairs are copiously created by an applied electric field near the Dirac point in graphene or similar two-dimensional electronic systems. It was shown recently that for sufficiently large electric fields E and ballistic times the I-V characteristics become strongly nonlinear due to Schwinger's pair creation rate, proportional to $E^{3/2}$. Since there is no energy gap the radiation from the pairs' annihilation is enhanced. The spectrum of radiation is calculated and exhibits a maximum at $\omega = \sqrt{eEv_g/\hbar}$. The angular and polarization dependence of the emitted photons with respect to the graphene sheet is quite distinctive. For very large currents the recombination rate becomes so large that it leads to the second Ohmic regime due to radiation friction.

DOI: 10.1103/PhysRevB.84.035414 PACS number(s): 72.80.Vp, 73.20.Mf, 12.20.−m

I. INTRODUCTION

Electronic mobility in graphene, especially one suspended on leads, is extremely large,[1] so that a graphene sheet is one of the purest electronic systems. The relaxation time of charge carriers due to scattering off impurities, phonons, ripplons, etc., in suspended graphene samples of sub-μm length is so large that the transport is ballistic.[2,3] The ballistic flight time in these samples can be estimated as $t_{\rm bal} = L/v_g$, where $v_g \simeq 10^6$ m/s is the graphene velocity characterizing the massless "ultrarelativistic" spectrum of graphene near Dirac points, $\varepsilon_k = v_g\,|\mathbf{k}|$, and L is the length of the sample that can exceed several μm.[4,5] The extraordinary physics appears right at the Dirac point at which the density of states vanishes. In particular, at this point graphene exhibits a quasi-Ohmic behavior, $\mathbf{J} = \sigma\mathbf{E}$, even in the purely ballistic regime.

A physical picture of this "resistivity" without either charge carriers or dissipation is as follows.[6] The electric field creates electron-hole excitations in the vicinity of the Dirac points similar to the Landau-Zener tunneling effect in narrow-gap semiconductors or electron-positron pair creation in quantum electrodynamics first studied by Schwinger[7] (later referred to as LZS). Importantly, in graphene the energy gap is zero thus the pair creation is possible at zero temperature and arbitrary small $\mathbf{E}$, even within linear response. Although the absolute value of the quasiparticle velocity v_g cannot be altered by the electric field due to the ultrarelativistic dispersion relation, the orientation of the velocity can be influenced by the applied field.The electric current $e\mathbf{v}$ proportional to the projection of the velocity $\mathbf{v}$ onto the direction of the electric field is increased by the field. These two sources of current, namely creation of moving charges by the electric field (polarization) and their reorientation (acceleration), are responsible for the creation of a stable current.

Agreement over the qualitative explanation notwithstanding, determination of the value of the minimal dc conductivity at the Dirac point in the limit of zero temperature had undergone a period of experimental and theoretical uncertainty. After the value in graphene on substrate was measured to be about $\sigma = 4e^2/h$,[8] it was shown in experiments on suspended samples[2] that the zero-temperature limit was not achieved and in fact that these early samples had too many charged "puddles," so that they represented an average around the neutrality or the Dirac point. The value in early-on suspended samples[2] was half of that and most recently settled at the "dynamical" $\sigma_2 = \frac{\pi}{2}\frac{e^2}{h}$ in best samples at 2 K temperature.[4] Theoretically several different values appeared. The value $\sigma_1 = \frac{4}{\pi}\frac{e^2}{h}$ had been considered as the "standard" one for several years[9] and appeared as a zero disorder limit in many calculations like the self-consistent harmonic approximation, although different regularizations within the Kubo formalism resulted in different values.[10]

The dynamical approach to transport was applied to the tight-binding model of graphene[11] to resolve this "regularization ambiguity." It consists of considering the ballistic evolution of the current density in time after a sudden or gradual switching on of the electric field. The result within linear response is that the current settles very fast, on the microscopic time scale of $t_\gamma = \hbar/\gamma \simeq 0.24$ fs (γ being the hopping energy), on the value of $J = \sigma_2 E$. The value is identical to the one obtained (at nonzero temperatures) for the ac conductivity.[12] The two contributions, polarization and attenuation, are comparable in strength and combine to produce a constant total current. However, a deeper analysis of the "quasi-Ohmic" graphene system beyond the leading order in perturbation theory in electric field revealed[13] that on the time scale

$$t_{nl} = \sqrt{\frac{\hbar}{eEv_g}} \tag{1}$$

the linear response breaks down. For larger times the quasi-Ohmic behavior no longer holds. This is in contrast to dissipative systems, in which the linear-response limit can be taken directly at infinite time. This perhaps is the origin of the "regularization" ambiguities in graphene, since large time and small field limits are different. The time scale

 ©2011 American Physical Society

on which nonlinear effects become dominant is not always very large; for example, in experiments dedicated to the breakdown of quantum Hall effect[14] in which $E = 10^4$ V/m, nonlinearity sets in at $t_{nl} = 0.3$ ps, that is, of order ballistics time for $L = 0.3$ μm. Graphene flakes under larger fields of order 2×10^6 V/m have been studied very recently (at room temperature) in specially designed high current density experiments.[5] In this case the nonlinear time is only 20 fs, much lower than the ballistic time $t_{\rm bal} = 2$ ps for $L = 2$ μm. Analytic and numerical solutions of the tight-binding model[13] as well as of the Dirac model describing the physics near the Dirac point demonstrated[13,15] that at t_{nl} the electron-hole pairs' creation becomes dominant and is well described by an adaptation of the well-known (nonanalytic in **E**) Schwinger electron-positron pair creation rate,

$$\frac{d}{dt}N_p = \frac{3^{3/4}}{2^{9/2}v_g^{1/2}}\left(\frac{eE}{\hbar}\right)^{3/2}. \tag{2}$$

The difference with the original derivation[7] in the context of particle physics is that the fermions are $2+1$ dimensional and "massless," thus magnifying the effect. The polarization current is $J(t) = 2ev_gN(t)$ and therefore Schwinger's creation rate leads to a linear increase with time:[13]

$$J(t) = \sigma_2\left(\frac{\sqrt{3}}{2}E\right)^{3/2}\left(\frac{ev_g}{\hbar}\right)^{1/2}t. \tag{3}$$

The physics of pair creation is highly nonperturbative and nonlinear in nature and therefore, instead of the linear response, Schwinger found an exact formula using functional methods. The rate can be intuitively understood using the much simpler instanton approach originally proposed in the context of particle physics[16] (extended later to low dimensions[17]), but is known in fact in condensed-matter physics as the Landau-Zener tunneling probability.[5,15,18] In particle physics it is extremely difficult to observe Schwinger's creation rate and it would be interesting to establish experimentally this dynamical phase in low dimensional condensed-matter physics featuring the massless Dirac quasiparticle spectrum like graphene or novel materials sharing with it the massless Dirac spectrum like topological insulators or tuned semiconductor heterojunctions.[19] Of course transport phenomena at rather large fields always have a background related to possible influence of leads, disorder, and thermal effects like local heating, etc.

In this paper we draw attention to a direct and unintrusive signature of the dynamical phase of LZS pair creation in a graphene sheet subject to an applied electric field. It is demonstrated that the flux of photons radiating from the surface of the sample is characterized by the creation rate since the photons are emitted via electron-hole pair annihilation and therefore proportional to $E^{3/2}$, a hallmark of Schwinger's process. In addition, the frequency, direction, and polarization characteristics of the radiation generated by the electric field calculated here all bear footprints of the pair creation dynamics.

II. ELECTRON-HOLE RECOMBINATION RATE INTO PHOTONS

A. Amplitude for emission of a single photon

The electrons and their electromagnetic interaction with photons are approximately described near a Dirac point by the Weyl Hamiltonian:

$$H = \int d^3r\ \psi^\dagger \begin{bmatrix} v_g\boldsymbol{\sigma}\cdot\left(-i\hbar\nabla + \frac{e}{c}\mathbf{A}\right) \\ -\frac{\hbar^2}{2m}\left(\partial_z + i\frac{e}{\hbar c}A_z\right)^2 + V_{\rm conf}(z) \end{bmatrix}\psi. \tag{4}$$

Here ψ is the two-component spinor second quantized field and $(\mathbf{A}, A_z)$ is the vector potential (bold letters describe vectors in the graphene plane, while z is the perpendicular direction). Electrons (charge $-e$) and holes (charge e) in the graphene sheet are confined in this model to the $z = 0$ plane by a potential $V_{\rm conf}$ (small shape changes can be neglected for our purposes). The only requirement from this potential is that it is strong enough to "freeze" the motion along the z direction. In the single graphene sheet one has two left-handed chirality Weyl fermions described by the above Hamiltonian in which $\boldsymbol{\sigma}$ denotes the in-plane Pauli matrices and two right-handed Weyl fermions represented by $\boldsymbol{\sigma}^\dagger$. To include the topological insulators case,[19] we first concern ourselves with only one spinor.

We consider the emission of a photon with wave vector $(\mathbf{k}, k_z)$ and frequency $\omega = c\sqrt{\mathbf{k}^2 + k_z^2}$, described by a linearly polarized plane wave,

$$\mathbf{A}_{ph} = \frac{2E_0}{\omega}\mathbf{e}^{(\lambda)}\sin\left(\mathbf{k}\cdot\mathbf{r} + k_z z - \omega t\right), \tag{5}$$

whereas the dc applied field is $\mathbf{A}_{\rm ext} = (0, -cEt)$. For regularization we make use of a finite box $L \times L \times L_z$, so that momenta are discrete and the single photon's electric field is $E_0^2 = \hbar\omega/(L^2L_z)$. The unit vectors

$$\begin{aligned} \mathbf{e}^{(1)} &= (-\sin\varphi, \cos\varphi); \quad e_z^{(1)} = 0; \\ \mathbf{e}^{(2)} &= -\cos\theta(\cos\varphi, \sin\varphi); \quad e_z^{(2)} = \sin\theta \end{aligned} \tag{6}$$

describe polarizations that are conveniently chosen similarly to a recent calculation of electromagnetic emission due to thermal fluctuations.[20] The vectors $\mathbf{e}^{(1)}$ and $\mathbf{e}^{(2)}$ represent the "in-plane" and the "out-of-plane" polarizations, respectively. The electron and the hole wave functions are $\frac{1}{\sqrt{2L}}e^{i\mathbf{p}\cdot\mathbf{r}}u(\mathbf{p})\psi_n(z)$ and $\frac{1}{\sqrt{2L}}e^{i\mathbf{p}'\cdot\mathbf{r}}v(\mathbf{p}')\psi_n(z')$, with spinors defined by

$$u(\mathbf{p}) = \begin{pmatrix} 1 \\ -ie^{i\phi} \end{pmatrix}; \quad v(\mathbf{p}') = \begin{pmatrix} 1 \\ ie^{i\phi'} \end{pmatrix}, \tag{7}$$

with $\mathbf{p} + \frac{e}{\hbar c}\mathbf{A}_{\rm ext} = p(\cos\phi, \sin\phi)$. $\psi_n(z)$ are wave functions of the confinement. The interaction with a photon at time t happens when the momentum is minimally shifted due to the dc field. The golden rule photon emission rate [for an "initial" electron with momentum $\mathbf{p}$ and a "final" hole $\mathbf{p}'$ and a photon of polarization λ and momentum $(\mathbf{k}, k_z)$] is

$$\begin{aligned} W_{nn'}^{(\lambda)}(\mathbf{p},\mathbf{p}',\mathbf{k},k_z,t) = \frac{2\pi}{\hbar}\left|F_{nn'}^{(\lambda)}\right|^2 N_{\mathbf{p}}(t)N_{-\mathbf{p}'}(t) \\ \times\delta[\hbar v_g(p+p') - \hbar\omega]. \end{aligned} \tag{8}$$

In terms of Feynman diagrams of quantum electrodynamics[21] it corresponds to the diagram in Fig. 1(a). Here $N_{\mathbf{p}}(t)$ is the density of electrons in a certain momentum range produced

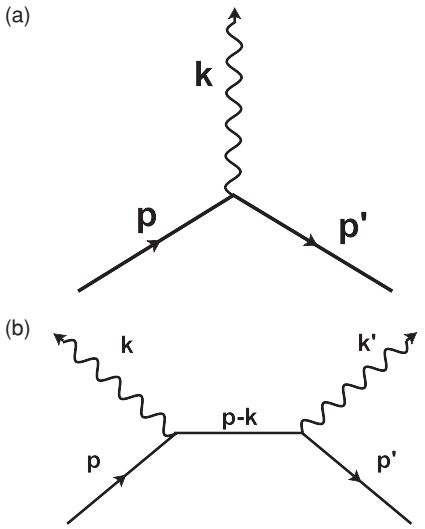

FIG. 1. Feynman diagrams representing the major electromagnetic processes in graphene. (a) One-photon emission. (b) Two-photon emission.

by the electric field $\mathbf{E}$, and $N_{-\mathbf{p}'}(t)$ is the density of holes (equal to that of the electrons at the opposite momentum due to particle-hole symmetry). The density calculated using the simple Landau-Zener creation rate expression for one of the flavors is[13,15,16]

$$N_{\mathbf{p}}(t) = \Theta(p_y)\Theta\left(\frac{e}{\hbar}Et - p_y\right)\exp\left(-\frac{\pi\hbar v_g}{eE}p_x^2\right), \quad (9)$$

where Θ are the Heaviside functions. The transition amplitude is given by

$$F_{nn'}^{(\lambda)} = i\frac{E_0}{\omega}\frac{ev_g}{2L^2}e^{i[v_g(p+p')-\omega]}\mathcal{F}_{\mathbf{p},\mathbf{p}'}^{(\lambda)} \times \int dz\, e^{ik_z z}\psi_n^*(z)\psi_{n'}(z)\delta(\mathbf{p}+\mathbf{p}'-\mathbf{k}), \quad (10)$$

where matrix elements $\mathcal{F}_{\mathbf{p},\mathbf{p}'}^{(\lambda)} \equiv v^\dagger(-\mathbf{p}')\boldsymbol{\sigma}\cdot\mathbf{e}^{(\lambda)}u(\mathbf{p})$ are

$$\left|\mathcal{F}_{\mathbf{p},\mathbf{p}'}^{(1)}\right|^2 = 2[1-\cos(2\varphi-\phi-\phi')]; \quad \left|\mathcal{F}_{\mathbf{p},\mathbf{p}'}^{(2)}\right|^2 = 2\cos^2\theta[1+\cos(2\varphi-\phi-\phi')]. \quad (11)$$

B. Spectral emittance

For tight confinement to the $z=0$ plane one should consider only the ground state $n=n'=0$. Note that the perpendicular component of the wave vector k_z is "free" from conservation that prohibits the process in fully relativistic QED.[21] The phase space for annihilation is very limited due to $v_g \ll c$, see Appendix A, and leads to important simplifications.

Let us define the spectral emittance per volume of the k space (and area of the graphene flake) as

$$\mathcal{M}^{(\lambda)}(\mathbf{k},k_z,t) = \frac{4\hbar\omega}{L^2}\sum_{\mathbf{p},\mathbf{p}'}\frac{d}{dk_z d\mathbf{k}}W^{(\lambda)}(\mathbf{p},\mathbf{p}',\mathbf{k},k_z,t) = \frac{e^2v_g^2}{(2\pi)^4}\int d\mathbf{p}\left|\mathcal{F}_{\mathbf{p},\mathbf{k}-\mathbf{p}}^{(\lambda)}\right|^2 N_{\mathbf{p}}N_{\mathbf{k}-\mathbf{p}} \times \delta(v_g(p+|\mathbf{k}-\mathbf{p}|)-\omega), \quad (12)$$

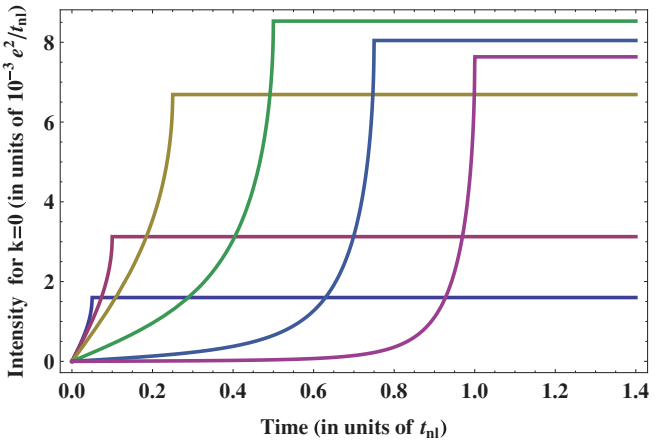

FIG. 2. (Color online) The spectral emittance in direction perpendicular to the graphene plane, $\mathbf{k}=0$. Polarizations are summed over. The emittance (in units of e^2/t_{nl}) for various frequencies (in units of t_{nl}^{-1}) as function of ballistic time from $0.1t_{nl}$ to $1.4t_{nl}$.

where the integration over $\mathbf{p}'$ was performed using the δ function expressing the conservation of momentum. We first study the frequency dependence of the radiation in the direction perpendicular to the graphene flake, $\mathbf{k}=\mathbf{0}$. Multiplying by 4 for the spin and valley degeneracy, summing over the polarizations ($\sum_\lambda |\mathcal{F}_{\mathbf{p},\mathbf{p}}^{(\lambda)}|^2 = 4$), and integrating over $\mathbf{p}$ one obtains, using $\omega = ck_z$, the spectral emittance

$$\mathcal{M}(\mathbf{k}=\mathbf{0},\omega,t) = \frac{e^2v_g^2t_{nl}^2}{\pi^4}\int_{-t/t_{nl}}^{0} d\overline{p}\,\Theta(t_{nl}\omega/2+\overline{p}) \times \frac{\exp\left[-2\pi\left(t_{nl}^2\omega^2/4-\overline{p}^2\right)\right]}{\omega\left(t_{nl}^2\omega^2/4-\overline{p}^2\right)^{1/2}}. \quad (13)$$

The spectral emittance, presented in Fig. 2 for various frequencies as a function of time, increases linearly for $t \ll \omega^{-1}$, $\mathcal{M}(\mathbf{k}=\mathbf{0},\omega,t) = \frac{2e^2t}{\pi^4t_{nl}^2}e^{-\pi t_{nl}^2\omega^2/2}$, then rises sharply approaching a maximum at $t=\omega t_{nl}^2/2$ and stabilizes at

$$\mathcal{M}(\mathbf{k}=\mathbf{0},\omega,t\gg t_{nl}) = \frac{e^2}{\pi^3}\omega e^{-\pi t_{nl}^2\omega^2/4}I_0\left(\frac{\pi t_{nl}^2\omega^2}{4}\right), \quad (14)$$

where I_0 is the modified Bessel function. The asymptotic value rises linearly with frequency, $\pi^{-3}\omega$, in the infrared, reaches its maximum at $\omega = t_{nl}^{-1}$, and falls slightly to $\frac{\sqrt{2}e^2}{\pi^4 t_{nl}}$ in the ultraviolet. In Fig. 3 the emittance at various ballistic times is given as function of frequency. For each ballistic time the curve has two parts. The first follows the universal dependence given by Eq. (14). Therefore the frequency for observation of the Schwinger effect, not surprisingly, should exceed $\omega_{\min} = \sqrt{eEv_g/\hbar}$, which amounts to 3.6 THz for $E = 10^4$ V/m, and 50 THz for $E = 2\times10^6$ V/m. At a higher frequency $\omega_{\max} = 2t/t_{nl}^2$ the emittance sharply drops. Therefore the frequency does not exceed $2t_{\rm bal}/t_{nl}^2$.

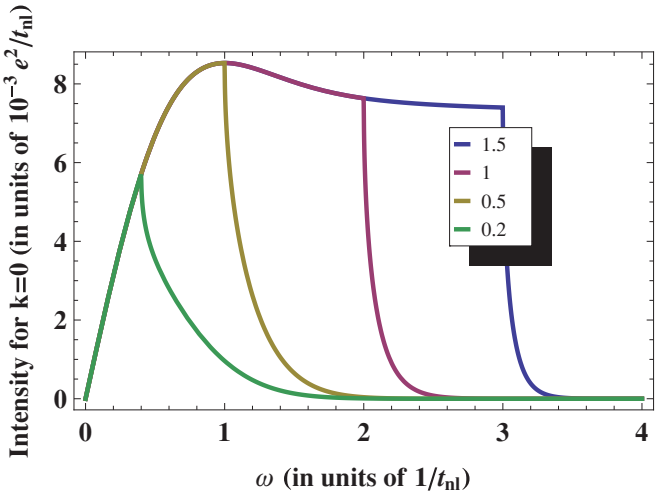

FIG. 3. (Color online) The emittance at various times (in units of t_{nl}) as function of frequency.

C. Angular and polarization distribution

Next we consider the angular and polarization dependence of the radiated power per unit area defined as the spectral intensity, Eq. (12), integrated over frequencies,

$$\mathcal{L}^{(\lambda)}(\theta,\varphi,t) \equiv \int_0^\infty d\omega \frac{\omega^2}{c^3} \mathcal{M}^{(\lambda)}\left(\mathbf{k}, \frac{\omega}{c}, t\right). \tag{15}$$

Performing integrations and simplifying, utilizing the small parameter $v \equiv v_g/c \simeq 1/300 \ll 1$, see Appendix B for details, one obtains

$$\mathcal{L}^{(1)}(\varphi,t) = \frac{e^4 v^4 E^2}{2^{5/2}\pi^4 c\hbar^2}\left(\frac{t}{4\pi t_{nl}}\cos^2\varphi + \frac{t^3}{3t_{nl}^3}\sin^2\varphi\right); \tag{16}$$

$$\mathcal{L}^{(2)}(\theta,\varphi,t) = \frac{e^4 v^4 E^2}{2^{5/2}\pi^4 c\hbar^2}\cos^2\theta \times \left(\frac{t}{4\pi t_{nl}}\sin^2\varphi + \frac{t^3}{3t_{nl}^3}\cos^2\varphi\right). \tag{17}$$

The radiant flux from a flake of a μm $\times$ μm size is 4.7×10^{-21} W, for $E = 10^4$ V/m corresponding to the emission rate of just 10 photons per second, yet for the high current samples[5] with $E = 2 \times 10^6$ V/m of the same area one gets a more significant output: the radiant flux is 1.3×10^{-17} W, corresponding to the emission rate of 3×10^4 photons per second.

The two quantities $\mathcal{L}^{(1,2)}$ and their sum are presented for $t = t_{nl}$ in the spherical plots of Figs. 4(a)–4(c), respectively. The radiated power is maximal in direction perpendicular to the graphene plane. For directions close to the azimuth angles $\varphi = 0^\circ$ and 180° (perpendicular to the electric field or current) at small polar angles θ (perpendicular to the graphene plane) the intensities of the two polarizations are of the same order, while for $\theta \sim 90^\circ$ (close to the in-plane direction) the out of plane polarization, $\lambda = 2$, dominates. On the other hand, for $0^\circ \ll \varphi \ll 180^\circ$ the picture is the opposite. As expected, the unpolarized intensity, Fig. 4(c), is less anisotropic; yet the radiation is somewhat depressed in the direction perpendicular to the current and close to the plane.

The two-photon processes, see Fig. 1(b), are suppressed by the factor $\alpha_{\rm QED} = \frac{e^2}{c\hbar} \approx \frac{1}{137}$ compared to the one-photon process due to an additional vertex, while the phase space of two diagrams is of the same order; see Appendix C for details.

III. DISCUSSION

Now we elaborate on a number of related issues and comment on the experimental feasibility of exploring the Schwinger phase physics. We start with a qualitative discussion of the rather unusual physics arising at strong applied fields, when the pair recombination becomes an important relaxation channel.

A. Coulomb interaction and the formation of the neutral electron-hole plasma

Even if the ballistic time and the relaxation time are very large, Schwinger's dynamical pair creation phase cannot persist for a long time at large field since density of charges (or both signs) becomes large. When the density of quasiparticles reaches the order of $\rho_p = 10^{11}$ cm^{-2} a neutral electron-hole plasma is created[22] (like in some semiconductor systems under irradiation). In this state electrostatic interactions (despite being screened at large distances) become dominant, as was discussed extensively in connection with electron-positron pairs creation in quantum electrodynamics.[21] When electrons and holes are close enough they strongly attract each other effectively facilitating the recombination process. The rate therefore far exceeds the one calculated within perturbation theory in Sec. III. Let us first estimate when this state is achieved at experimentally accessible situations.

Assuming the Schwinger pair creation rate, Eq. (2), the density will approach ρ_p at times of order $t_p \propto \rho_p/E^{3/2}$. With a moderate field value of $E = 10^4$ V/m,[14] the "plasma time" $t_p = 140$ ps $\simeq 400 t_{nl}$ exceeds the ballistic time of the $L = 1$-μm-long sample (and probably also the relaxation time in current experiments on graphene). Yet with higher achievable fields $E = 2 \times 10^6$ V/m,[5] the plasma time is reduced to $t_p = 40$ fs $\simeq 2\ t_{nl} \ll t_{\rm bal}$, so that the "radiation friction" dissipation channel opens up: electron-hole pairs annihilate emitting photons, which take energy out of the graphene sheet and thus a different Ohmic behavior is reached. This is roughly the ballistic time range for which the emission was calculated in Sec. III. Of course, due to the Coulomb attraction enhancement of the recombination the intensity becomes grossly underestimated in the plasma regime. The pair density will have to be recalculated via Boltzmann equations; this will be done in a separate publication. One, however, might expect qualitatively that this conductivity in the "second" Ohmic regime certainly exceeds σ_2 and is likely to reach several times σ_2. Data presented in Ref. 5 for *clean* samples, see Figs. 3 and 12 therein, are consistent with the linear (Ohmic) I-V curve at such conductivity value. However, the experimental situation in the transport experiment is rather complex, as discussed next.

B. Experimental evidence of the pair creation in samples of mesoscopic size

In this subsection we use the above radiation-friction scenario to discuss whether there is a clear and unambiguous

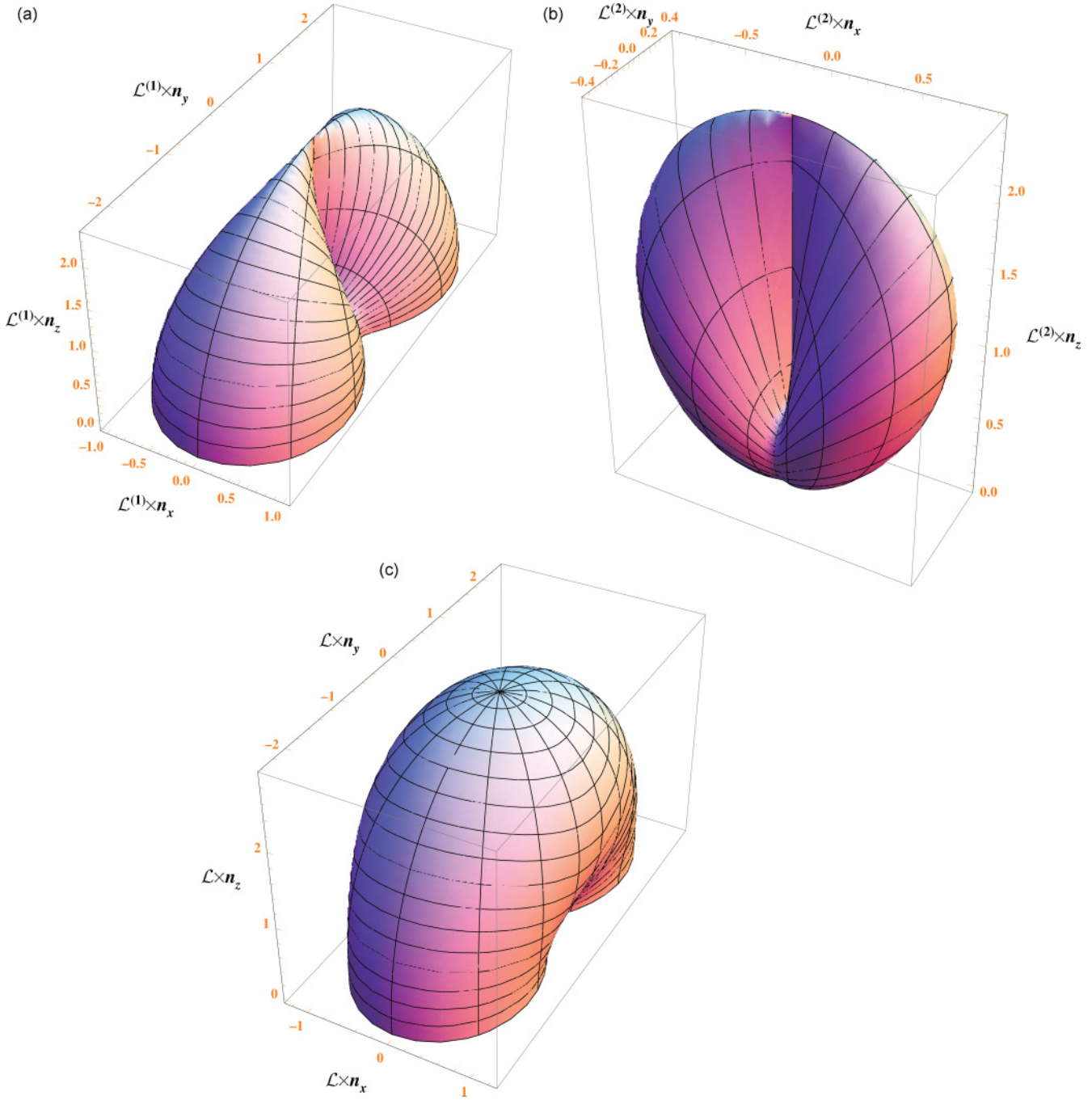

FIG. 4. (Color online) (a) The angle dependence of the intensity as function of the photon spherical angles φ,θ (half of the whole solid angle). Time is fixed at $t = t_{nl}$. In-plane polarization. (b) Out-of-plane polarization. (c) Unpolarized light.

signature of the Schwinger's pair creation phase in transport experiments. In a series of remarkable experiments the nonlinear I-V were measured at high electric fields of the order 2×10^6 V/m at room temperature.[5] The samples were treated in such a way that, despite being nonsuspended, the typical charge asymmetry did not appear and the Dirac point was accessed convincingly at zero gate voltage (this demonstrates high quality and is in variance with most samples on substrate). The I-V curves were studied in various high and low mobility samples [up to $\mu = 7000$ cm^2/ (Vs)] and effects of disorder were partially controlled by irradiating the samples. The samples were $L = 1$–2 μm long and rather narrow ($W = 0.5$ μm) and the four-probe technique was applied. Although a nonlinear I-V dependence $I \propto V^\alpha$ with exponent $\alpha = 1.3$–1.5 was observed at the Dirac point, surprisingly the nonlinearity disappeared in the highest mobility samples. In these experiments the ballistic time $t_{\rm bal} = 2$ ps is much larger than $t_{nl} = 20$ fs at the highest applied voltage of 4 V. Unfortunately the crossover voltages, namely when $t_{nl}\,(V) = t_{\rm bal}$ or

$$V_{nl} = \frac{\hbar v_g}{eL} = 0.32 \text{ mV}, \tag{18}$$

were not probed since at room temperature $k_B T = 25$ meV. As argued in the previous subsection the radiation friction causes a second Ohmic regime and the I-V curve in the clean samples is expected to be linear. It is disorder that might have caused the observed nonlinearity in irradiated samples. This requires an additional theoretical study that includes the effect of pair recombination. As argued above it becomes as important as the Landau-Zener-Schwinger pair creation process at such currents.

IV. CONCLUSIONS

To summarize, electron-hole pairs are copiously created via the Landau-Zener-Schwinger mechanism near the Dirac points in graphene or similar 2D electronic systems by an applied electric field, provided the available ballistic time exceeds t_{nl}, Eq. (1). The recombination into photons produces a characteristic signal proportional to $E^{3/2}$ at frequencies of order t_{nl}^{-1}, which enables unintrusive and unambiguous experimental observation of the Schwinger phenomenon. The angular and polarization dependence of the emitted photons with respect to the graphene sheet was calculated. At very high currents and sufficiently long ballistic times the recombination process becomes greatly enhanced by the electron-hole attraction and the radiation becomes an effective channel of dissipation, the radiation friction.

The calculation can be trivially extended to any system with a Dirac-point-like spectrum as double layer graphene and the recently synthesized family of materials called "topological insulators"[19] in which surface excitations are similar to those in graphene with the notable exception of chirality. Schwinger's mechanism is also expected in these materials since the mechanism does not involve chirality (left and right movers contribute equally to the emission rate of graphene). These materials have an advantage of not being strictly two dimensional, although ballistic times might be shorter at present. The driving current should not necessarily be dc; a sufficient condition is $\omega_{\rm ext} \ll t_{nl}^{-1}$. Detectors of light (photon counters) in the microwave infrared that are sensitive enough have recently been developed.[23] Hopefully Schwinger's pair creation rate formula can be directly tested using condensed-matter materials endowed with relativistic fermion spectra.

ACKNOWLEDGMENTS

We are indebted to E. Farber and W. B. Jian, J. Pan for valuable discussions. Work of B.R. and H.K. was supported by NSC of R.O.C. Grants No. 98-2112-M-009-014-MY3 and No. 98-2112-M-003-002-MY3, respectively, the National Center for Theoretical Sciences, and the MOE ATU program. H.K. acknowledges the hospitality of the Physics Department of AUCS, while M.L. acknowledges the hospitality and support of the NCTS.

APPENDIX A: PHASE SPACE OF THE ONE-PHOTON PROCESS

Planar electrons and holes are described by their momenta $\mathbf{p}$ and $\mathbf{p}'$ in the x-y plane [see Sec. II A for notations], while the momentum of the photon k is three dimensional. The conservation of the in-plane momentum and the conservation of energy read

$$\mathbf{p} + \mathbf{p}' = \mathbf{k}; \quad v_g(p + p') = ck. \tag{A1}$$

The momentum in the z direction is not conserved; it is balanced by the elasticity of the graphene flake. Since $k = \sqrt{k_z^2 + |\mathbf{k}|^2} \geqslant |\mathbf{k}|$, in terms of $\mathbf{p}$ and $\mathbf{p}'$ one has the inequality

$$v^2(p + p')^2 - |\mathbf{p} + \mathbf{p}'|^2 \geqslant 0, \tag{A2}$$

or, in the polar coordinates,

$$(1 - v^2)(p^2 + p'^2) + 2[\cos(\phi - \phi') - v^2]pp' \leqslant 0. \tag{A3}$$

With the above constraint the condition that p' has real solutions leads to

$$\cos(\phi - \phi') \leqslant -1 + 2v^2. \tag{A4}$$

As $v \ll 1$, it is obvious that $\phi' - \phi$ is very close to π. By defining $\Delta\phi = \pi - (\phi' - \phi)$, one sees that the above condition simplifies to

$$-2v \leqslant \Delta\phi \leqslant 2v. \tag{A5}$$

Substituting the above result back into Eq. (A3) it can be seen that p' is very close to p. By introducing $\Delta r = 1 - p'/p$, the condition becomes

$$\Delta r^2 + \Delta\phi^2 \leqslant 4v^2. \tag{A6}$$

Therefore the allowed region is a disk of radius $2v$.

APPENDIX B: DERIVATION OF THE AMPLITUDE AND SPECTRAL EMITTANCE

The golden rule photon emission rate [for an "initial" electron with momentum $\mathbf{p}$, a "final" hole $\mathbf{p}'$ and a photon of polarization λ and momentum $(\mathbf{k}, k_z)$] is given by Eq. (8). Correspondingly the rate defined in Eq. (12) is

$$\begin{aligned}\mathcal{M}^{(\lambda)}&\left(\theta, \varphi, \frac{\omega}{c}, t\right) \\ &= \frac{e^2 v_g^2}{(2\pi)^4} \int d\mathbf{p} \left|\mathcal{F}^{(\lambda)}_{\mathbf{p},\mathbf{k}-\mathbf{p}}\right|^2 N_{\mathbf{p}} N_{\mathbf{k}-\mathbf{p}} \delta[v_g(p + |\mathbf{k} - \mathbf{p}|) - \omega] \\ &= \frac{e^2 v_g^2}{(2\pi)^4} \int p\,(\phi)\, d\phi \left|\mathcal{F}^{(\lambda)}_{\mathbf{p},\mathbf{k}-\mathbf{p}}\right|^2 N_{\mathbf{p}} N_{\mathbf{k}-\mathbf{p}} \cdot J(\phi).\end{aligned} \tag{B1}$$

Because of the δ function, the integration over $\mathbf{p}$ imposes the condition of energy conservation. As a result, the squares of the matrix elements, Eq. (11) simplify:

$$\begin{aligned}\left|\mathcal{F}^{(1)}_{\mathbf{p},\mathbf{p}'}\right|^2 &= \frac{4[\cos(\phi - \varphi) - v\sin\theta]^2}{[1 - 2v\sin\theta\cos(\phi - \varphi) + v^2\sin^2\theta]}; \\ \left|\mathcal{F}^{(2)}_{\mathbf{p},\mathbf{p}'}\right|^2 &= \frac{4\cos^2\theta\sin^2(\phi - \varphi)}{[1 - 2v\sin\theta\cos(\phi - \varphi) + v^2\sin^2\theta]}.\end{aligned} \tag{B2}$$

Moreover, there is an additional factor from the δ function:

$$J(\phi) = \frac{[1 - 2v\sin\theta\cos(\phi - \varphi) + v^2\sin^2\theta]}{2v_g[1 - 2v\sin\theta\cos(\phi - \varphi)]^2}. \tag{B3}$$

The Jacobian of the transition to polar coordinates is

$$p(\phi) = \frac{\omega(1 - v^2\sin^2\theta)}{2v_g[1 - 2v\sin\theta\cos(\phi - \varphi)]}. \tag{B4}$$

In view of the step functions for the LZS density, Eq. (9), the following possibilities occur.

Into the forward direction (positive projection on the electric field) $0 < \varphi < \pi$. The conditions imposed by the step functions are $0 < -p_y$ and $0 < \frac{eE}{\hbar}t + p_y - k_y$. In terms of the polar coordinates in the momentum space, the following apply:

(i) for $0 < \frac{2t}{\omega t_{nl}^2} < 1 + v\sin\theta\sin\varphi$, the allowed regions are $\Delta_+ - \phi_0 < \phi < 0$ or $-\pi < \phi < -\pi + \phi_0 - \Delta_+$, with

$$\phi_0 = \arcsin\left(\frac{2t}{\omega t_{nl}^2}\right),$$
$$\Delta_+ = v\sin\theta\tan\phi_0\left[\cos(\varphi+\phi_0) + 2\sin\varphi\csc\phi_0\right]. \tag{B5}$$

(ii) for $1 + v\sin\theta\sin\varphi < \frac{2t}{\omega t_{nl}^2}$, the allowed region for ϕ is $-\pi < \phi < 0$.

Into the backward direction (negative projection on the electric field) $-\pi < \varphi < 0$. The conditions imposed by the step functions now become $0 < -p_y + k_y$ and $0 < \frac{eE}{\hbar}t + p_y$. In terms of the polar coordinates in the momentum space, the following apply:

(i) for $-2v\sin\theta\sin\varphi < \frac{2t}{\omega t_{nl}^2} < 1 - v\sin\theta\sin\varphi$, the allowed regions are $-(\phi_0 - \Delta_-) < \phi < 2v\sin\theta\sin\varphi$ or $-\pi - 2v\sin\theta\sin\varphi < \phi < -\pi + \phi_0 - \Delta_-$, where

$$\Delta_- = v\sin\theta\tan\phi_0\cos(\varphi+\phi_0). \tag{B6}$$

(ii) for $1 - v\sin\theta\sin\varphi < \frac{2t}{\omega t_{nl}^2}$, the allowed region for ϕ is $-\pi - 2v\sin\theta\sin\varphi < \phi < -2v\sin\theta\sin\varphi$.

Since $v \equiv v_g/c \simeq 1/300 \ll 1$, one can neglect higher-order correction in v. The conditions for case (i) simplify into $0 < \frac{2t}{\omega t_{nl}^2} < 1$ and $-\phi_0 < \phi < 0$ or $-\pi < \phi < -\pi + \phi_0$. Therefore

$$\mathcal{M}^{(1)}\left(\theta,\varphi,\frac{\omega}{c},t\right) = \frac{e^2\omega}{8\pi^4}\int_0^{\phi_0} d\phi(\cos^2\phi\cos^2\varphi + \sin^2\phi\sin^2\varphi) \times \exp\left[-\frac{\pi}{2}\omega^2 t_{nl}^2\cos^2\phi\right];$$
$$\mathcal{M}^{(2)}\left(\theta,\varphi,\frac{\omega}{c},t\right) = \frac{e^2\cos^2\theta}{8\pi^4}\int_0^{\phi_0} d\phi(\cos^2\phi\sin^2\varphi + \sin^2\phi\cos^2\varphi) \times \exp\left[-\frac{\pi}{2}\omega^2 t_{nl}^2\cos^2\phi\right]. \tag{B7}$$

Similarly, the conditions for case (ii) simplify: $\frac{2t}{\omega t_{nl}^2} > 1$ and $-\pi < \phi < 0$. Thus

$$\mathcal{M}^{(1)}\left(\theta,\varphi,\frac{\omega}{c},t\right) = \frac{e^2}{16\pi^4}\omega\int_{-\pi}^{0} d\phi\cos^2(\phi-\varphi)\exp\left[-\frac{\pi}{2}t_{nl}^2\omega^2\cos^2\phi\right] = \frac{e^2}{32\pi^3}\omega e^{-\pi t_{nl}^2\omega^2/4}\left[I_0\left(\frac{\pi t_{nl}^2\omega^2}{4}\right) - \cos 2\varphi I_1\left(\frac{\pi t_{nl}^2\omega^2}{4}\right)\right];$$
$$\mathcal{M}^{(2)}\left(\theta,\varphi,\frac{\omega}{c},t\right) = \frac{e^2}{16\pi^4}\omega\cos^2\theta\int_{-\pi}^{0} d\phi\sin^2(\phi-\varphi)\exp\left[-\frac{\pi}{2}t_{nl}^2\omega^2\cos^2\phi\right] = \frac{e^2}{32\pi^3}\omega e^{-\pi t_{nl}^2\omega^2/4}\cos^2\theta\left[I_0\left(\frac{\pi t_{nl}^2\omega^2}{4}\right) + \cos 2\varphi I_1\left(\frac{\pi t_{nl}^2\omega^2}{4}\right)\right]. \tag{B8}$$

These expressions lead to the final results for the spectral emittance Eqs. (13) and (14).

Next we consider the angular and polarization dependence of the radiated power per unit area defined as the spectral intensity $\mathcal{L}^{(\lambda)}(\theta,\varphi,t)$, Eq. (15). In the above formulas one can first integrate over ω in the range $0 < \omega < \frac{2t}{t_{nl}^2}\csc\phi$, and then integrate over ϕ in the region $[0,\frac{\pi}{2}]$. This leads to Eqs. (16) and (17) for the luminosity integrated over frequencies.

APPENDIX C: PHASE SPACE OF THE TWO-PHOTON PROCESS

As in QED,[21] the two-photon diagram, Fig. 1(b), gives rise to the following S-matrix element

$$F_2^{(\lambda,\lambda')}(p,p',k,k') = \frac{ie^2}{4\sqrt{\omega\omega'\varepsilon\varepsilon'}}\mathcal{F}_2^{(\lambda,\lambda')}(2\pi)^4\delta[v_g(p+p') - c(k+k')], \tag{C1}$$

where

$$\mathcal{F}_2^{(\lambda,\lambda')} = v^\dagger(-\mathbf{p}')\Xi^{(\lambda,\lambda')}u(\mathbf{p}) \tag{C2}$$

and

$$\Xi^{(\lambda,\lambda')} = (v\boldsymbol{\sigma}\cdot\mathbf{e}'^{(\lambda')})i\frac{(k-p') - \boldsymbol{\sigma}\cdot(\mathbf{k}-\mathbf{p}')}{v[(k-p')^2 - (\mathbf{k}-\mathbf{p}')^2]}(v\boldsymbol{\sigma}\cdot\mathbf{e}^{(\lambda)}) + (v\boldsymbol{\sigma}\cdot\mathbf{e}^{(\lambda)})i\frac{(p-k) - \boldsymbol{\sigma}\cdot(\mathbf{p}-\mathbf{k})}{v[(p-k)^2 - (\mathbf{p}-\mathbf{k})^2]}(v\boldsymbol{\sigma}\cdot\mathbf{e}'^{(\lambda')}).$$

The outcome of the integral in Eq. (12) is dictated by the size of the phase space and by the powers of the small parameters $v = v_g/c$ and $\alpha_{\mathrm{QED}} = e^2/(\hbar c)$. The power of v is the same as in the one-photon case, see Eq. (10). Yet there appears an additional power of α_{QED}.

Let us estimate the phase space. The conservation of momentum and energy for the two-photon process imply that

$$\mathbf{p} + \mathbf{p}' = \mathbf{k} + \mathbf{k}'; \quad v_g(p+p') = c(k+k'). \tag{C3}$$

Since $(k+k')^2 \geqslant (k_x+k_x')^2 + (k_y+k_y')^2$ one still has the inequality $v^2(p+p')^2 - |\mathbf{p}+\mathbf{p}'|^2 \geqslant 0$. Just like in the one-photon case (Appendix A), utilizing $v \ll 1$ leads to the constraints $\phi - \phi' \approx \pi$ and $p' \approx p$. The phase space of the two-photon case is thus roughly of the same order as that of the one-photon process. Therefore this two-photon process can be neglected.

*vortexbar@yahoo.com

[1]S. V. Morozov, K. S. Novoselov, M. I. Katsnelson, F. Schedin, D. Elias, J. A. Jaszczak, and A. K. Geim, Phys. Rev. Lett. **100**, 016602 (2008).

[2]X. Du, I. Skachko, A. Barker, and E. Y. Andrei, Nat. Nanotechnol. **3**, 491 (2008).

[3]K. I. Bolotin, K. J. Sikes, J. Hone, H. L. Stormer, and P. Kim, Phys. Rev. Lett. **101**, 096802 (2008).

[4]E. A. Andrei, *Talk at Workshop on Nonequilibrium Phenomana*, Kanpur, January 2010.

[5]A. Barreiro, M. Lazzeri, J. Moser, F. Mauri, and A. Bachtold, Phys. Rev. Lett. **103**, 076601 (2009); N. Vandecasteele, A. Barreiro, M. Lazzeri, A. Bachtold, and F. Mauri, Phys. Rev. B **82**, 045416 (2010).

[6]L. Fritz, J. Schmalian, M. Muller, and S. Sachdev, Phys. Rev. B **78**, 085416 (2008).

[7]J. Schwinger, Phys. Rev. **82**, 664 (1951); S. P. Kim, H. K. Lee, and Y. Yoon, Phys. Rev. D **78**, 105013 (2008).

[8]K. S. Novoselov, A. K. Geim, S. V. Morozov, D. Jiang, M. I. Katsnelson, I. V. Grigorieva, S. V. Dubonos, and A. A. Firsov, Nature (London) **438**, 197 (2005); Y. Zhang, Y. W. Tan, H. L. Stormer, and P. Kim, *ibid*. **438**, 201 (2005).

[9]A. H. Castro Neto, F. Guinea, N. M. R. Peres, K. S. Novoselov, and A. K. Geim, Rev. Mod. Phys. **81**, 109 (2009); N. M. R. Peres, *ibid*. **82**, 2673 (2010).

[10]K. Ziegler, Phys. Rev. Lett. **97**, 266802 (2006); Phys. Rev. B **75**, 233407 (2007).

[11]M. Lewkowicz and B. Rosenstein, Phys. Rev. Lett. **102**, 106802 (2009).

[12]L. A. Falkovsky and A. A. Varlamov, Eur. Phys. J. B **56**, 281 (2007).

[13]H. C. Kao, M. Lewkowicz, and B. Rosenstein, Phys. Rev. B **82**, 035406 (2010); B. Rosenstein, M. Lewkowicz, H. C. Kao, and Y. Korniyenko, *ibid*. **81**, 041416(R) (2010).

[14]V. Singh and M. M. Deshmukh, Phys. Rev. B **80**, 081404(R) (2009).

[15]B. Dora and R. Moessner, Phys. Rev. B **81**, 165431 (2010).

[16]A. Casher, H. Neuberger, and S. Nussinov, Phys. Rev. D **20**, 179 (1979); D. Allor, T. D. Cohen, and D. A. McGady, *ibid*. **78**, 096009 (2008).

[17]S. P. Gavrilov and D. M. Gitman, Phys. Rev. D **53**, 7162 (1996); S. P. Kim and D. N. Page, *ibid*. **65**, 105002 (2002); T. D. Cohen and D. A. McGady, *ibid*. **78**, 036008 (2008).

[18]D. Patane, L. Amico, A. Silva, R. Fazio, and G. E. Santoro, Phys. Rev. B **80**, 024302 (2009).

[19]B. A. Bernevig, T. L. Hughes, and S-C. Zhang, Science **314**, 1757 (2006); X-L. Qi and S-C. Zhang, Phys. Today **63**, 33 (2010); C. Brüne, A. Roth, E. G. Novik, M. König, H. Buhmann, E. M. Hankiewicz, W. Hanke, J. Sinova, and L. W. Molenkamp, Nat. Phys. **6**, 448 (2010); L. B. Zhang, K. Chang, X. C. Xie, H. Buhmann, and L. W. Molenkamp, New J. Phys. **12**, 083058 (2010).

[20]M. Mecklenburg, J. Woo, and B. C. Regan, Phys. Rev. B **81**, 245401 (2010).

[21]A. I. Ahiezer and V. B. Beresteckiy, *Quantum Electrodynamics* (Nauka, Moscow, 1981).

[22]O. G. Balev, F. T. Vasko, and V. Ryzhii, Phys. Rev. B **79**, 165432 (2009).

[23]B. E. Kardynał, S. S. Hees, A. J. Shields, C. Nicoll, I. Farrer, and D. A. Ritchie, Appl. Phys. Lett. **90**, 181114 (2007); H. Shibata, H. Takesue, T. Honjo, T. Akazaki, and Y. Tokura, *ibid*. **97**, 212504 (2010); T. Ueda and S. Komiyama, Sensors **10**, 8411 (2010); T. Yamashita, S. Miki, W. Qiu, M. Fujiwara, M. Sasaki, and Z. Wang, Appl. Phys. Express **3**, 102502 (2010).